

The Impact of Beam Broadening on the Quality of Radar Polarimetric Data

ALEXANDER V. RYZHKOV

Cooperative Institute for Mesoscale Meteorological Studies, University of Oklahoma, and NOAA/OAR/National Severe Storms Laboratory, Norman, Oklahoma

(Manuscript received 19 January 2006, in final form 17 August 2006)

ABSTRACT

The impact of beam broadening on the quality of radar polarimetric data in the presence of nonuniform beam filling (NBF) is examined both theoretically and experimentally. Cross-beam gradients of radar reflectivity Z , differential reflectivity Z_{DR} , and differential phase Φ_{DP} within the radar resolution volume may produce significant biases of Z_{DR} , Φ_{DP} , and the cross-correlation coefficient ρ_{hv} . These biases increase with range as a result of progressive broadening of the radar beam. They are also larger at shorter radar wavelengths and wider antenna beams.

Simple analytical formulas are suggested for estimating the NBF-induced biases from the measured vertical and horizontal gradients of Z , Z_{DR} , and Φ_{DP} . Analysis of polarimetric data collected by the KOUN Weather Surveillance Radar-1988 Doppler (WSR-88D) demonstrates that frequently observed perturbations of the radial Φ_{DP} profiles and radially oriented “valleys” of ρ_{hv} depression can be qualitatively and quantitatively explained using the suggested NBF model.

1. Introduction

The Joint Polarization Experiment (JPOLE) and other validation studies demonstrate superior performance of dual-polarization radar for rainfall estimation and radar echo classification (e.g., Ryzhkov et al. 2005a). These polarimetric products, however, have been validated at relatively close distances from the radar. To our knowledge, the maximal distance at which polarimetric analysis and/or classification was ever verified using in situ measurements is 120 km (Loney et al. 2002). In most studies, the largest range to which polarimetric rainfall estimation was tested with rain gauges does not exceed 100 km (e.g., Brandes et al. 2001, 2002; May et al. 1999; Le Bouar et al. 2001; Ryzhkov et al. 2005b). On the other hand, Giangrande and Ryzhkov (2003) and Ryzhkov et al. (2005a) show that although the polarimetric method for rain measurements still outperforms the conventional one beyond 100 km from the radar, the degree of improvement decreases with distance.

Progressive beam broadening and stronger impact of nonuniform beam filling (NBF) is one of the reasons

why the quality of polarimetric information deteriorates with range. Beam broadening is a common problem for both polarimetric and conventional (nonpolarimetric) radar. The issue of the vertical profile of reflectivity (VPR) correction for precipitation measurements with conventional radar is addressed in extended literature (see, e.g., the overview in Meischner 2004). Much less effort has been made to assess similar problems regarding polarimetric variables such as the differential reflectivity Z_{DR} , the differential phase Φ_{DP} , the specific differential phase K_{DP} , the depolarization ratio LDR, and the cross-correlation coefficient ρ_{hv} .

Adverse effects of NBF on polarimetric measurements are further exacerbated if the antenna patterns for horizontal and vertical polarizations are not identical. Theoretical formulas for the Z_{DR} , LDR, and ρ_{hv} biases caused by the antenna pattern mismatch are presented in the book by Bringi and Chandrasekar (2001). The errors in Z_{DR} due to mismatched copolar patterns together with intrinsic reflectivity gradients across the beam can be quite high at the periphery of strong storm cores (Herzegg and Carbone 1984; Pointin et al. 1988).

NBF may also cause significant perturbations of the radial profile of the differential phase (Ryzhkov and Zrnich 1998; Gosset 2004). Such perturbations of Φ_{DP} result in spurious values of its radial derivative K_{DP} and strong biases in the K_{DP} -based estimates of the rain

Corresponding author address: Alexander V. Ryzhkov, CIMMS/NSSL, 120 David L. Boren Blvd., Norman, OK 73072.
E-mail: Alexander.Ryzhkov@noaa.gov

rate. These adverse effects are commonly manifested as the appearance of negative K_{DP} in the regions of strongly nonuniform precipitation and become more pronounced as the physical size of the radar resolution volume increases at longer distances.

The magnitude of the cross-correlation coefficient ρ_{hv} is closely related to the distribution of the differential phase within the radar resolution volume. Large cross-beam gradients of Φ_{DP} may cause noticeable decrease of ρ_{hv} , which is, in its turn, accompanied by higher statistical errors in the measurements of all polarimetric variables (Ryzhkov 2005).

Strong vertical gradients of radar variables are commonly observed in the presence of the bright band in startiform rain. Beam broadening causes notable smearing of the brightband polarimetric signatures at the distances as close as 40–50 km from the radar (Giangrande et al. 2005). Such a smearing makes polarimetric classification of the melting layer more difficult, and estimation of rainfall becomes a challenge.

In this paper, we attempt to quantify the effects of beam broadening on polarimetric measurements using a simple model of NBF. We assume that the antenna patterns at the two orthogonal polarizations are perfectly matched and the biases of the measured Z_{DR} , Φ_{DP} , and ρ_{hv} are solely due to linear cross-beam gradients of different radar variables. In section 2, closed-form analytical solutions for the biases are obtained using this simplified model of gradients and the Gaussian antenna pattern. Section 3 contains analysis of the cross-beam gradients and the corresponding biases estimated from real data collected with the polarimetric prototype of the S-band Weather Surveillance Radar-1988 Doppler (WSR-88D) in Oklahoma. In section 4, we simulate the smearing effect of beam broadening on the polarimetric signatures of the melting layer for different antenna beamwidths and compare results of simulations with observational data. Finally, in section 5 we discuss practical implications of the observed effects.

2. Theoretical analysis

In the case of weather scatterers, the voltage vectors of the transmitted (\mathbf{V}^t) and received (\mathbf{V}) waves are related as

$$\begin{pmatrix} V_h \\ V_v \end{pmatrix} = C_1 \begin{pmatrix} T_{hh} & 0 \\ 0 & T_{vv} \end{pmatrix} \begin{pmatrix} S_{hh} & S_{hv} \\ S_{hv} & S_{vv} \end{pmatrix} \begin{pmatrix} T_{hh} & 0 \\ 0 & T_{vv} \end{pmatrix} \begin{pmatrix} V_h^t \\ V_v^t \end{pmatrix}, \quad (1)$$

where matrix elements S_{hh} , S_{vv} , and S_{hv} represent back-scattering coefficients of hydrometeors in the radar

resolution volume and T_{hh} and T_{vv} describe phase shifts and attenuations for H and V waves along the propagation path:

$$T_{hh} = \exp(-j\Phi_h - \Gamma_h), \quad (2)$$

$$T_{vv} = \exp(-j\Phi_v - \Gamma_v), \quad (3)$$

where $\Phi_{h,v}$ is the phase shift and $\Gamma_{h,v}$ is the attenuation. The differential phase Φ_{DP} is defined as

$$\Phi_{DP} = 2(\Phi_h - \Phi_v). \quad (4)$$

The coefficient C_1 is a constant depending on radar parameters and range from the scatterers (see the appendix). If both H and V waves are transmitted simultaneously [i.e., $\mathbf{V}^t = (V^t, V^t)$], then

$$V_h = C_1(T_{hh}^2 S_{hh} + T_{hh} T_{vv} S_{hv}) V^t, \quad (5)$$

$$V_v = C_1(T_{vv}^2 S_{vv} + T_{hh} T_{vv} S_{hv}) V^t. \quad (6)$$

In our analysis we will neglect the cross-coupling terms proportional to S_{hv} in (5)–(6), which is reasonable assumption for rain and aggregated snow (Doviak et al. 2000).

Using (5) and (6), we introduce effective radar reflectivity factors $Z_{h,v}^{(e)}$ at orthogonal polarizations as

$$Z_h^{(e)} = C_2 \overline{|V_h|^2} = Z_h e^{-4\Gamma_h} \quad (7)$$

and

$$Z_v^{(e)} = C_2 \overline{|V_v|^2} = Z_v e^{-4\Gamma_v}, \quad (8)$$

the effective differential reflectivity

$$Z_{dr}^{(e)} = \frac{Z_h^{(e)}}{Z_v^{(e)}} = Z_{dr} e^{-4(\Gamma_h - \Gamma_v)}, \quad (9)$$

and the covariance

$$R_{hv} = C_2 \overline{V_h^* V_v} = Z_{hv} e^{j\Phi_{DP}}, \quad (10)$$

where

$$Z_{hv} = (Z_h Z_v)^{1/2} |\rho_{hv}| e^{-2(\Gamma_h + \Gamma_v)} \quad \text{and} \quad \Phi_{DP} = \Phi_{DP} + \arg(\rho_{hv}). \quad (11)$$

In (7)–(11), intrinsic values of the radar reflectivities $Z_{h,v}$, the differential reflectivity Z_{dr} , and the cross-correlation coefficient ρ_{hv} are defined from the second moments of the scattering matrix \mathbf{S} :

$$Z_h = C' \langle |S_{hh}|^2 \rangle, \quad Z_v = C' \langle |S_{vv}|^2 \rangle, \quad Z_{dr} = \frac{\langle |S_{hh}|^2 \rangle}{\langle |S_{vv}|^2 \rangle},$$

$$\rho_{hv} = \frac{\langle S_{hh}^* S_{vv} \rangle}{\langle |S_{hh}|^2 \rangle^{1/2} \langle |S_{vv}|^2 \rangle^{1/2}}. \quad (12)$$

Overbars in (7), (8), and (10) mean expected values and brackets in (12) stand for ensemble averaging. The factors C_2 and C' are constants defined in the appendix. In the absence of propagation effects and cross coupling, the effective reflectivity factors are equal to their intrinsic values.

The radar-measured reflectivities $Z_{h,v}^{(m)}$ and the covariance $R_{hv}^{(m)}$ are weighted by the radar antenna pattern $I(\mathbf{r}, \mathbf{r}_0)$ as follows (see the appendix for details):

$$Z_{h,v}^{(m)}(\mathbf{r}_0) = \int Z_{h,v}^{(e)}(\mathbf{r})I(\mathbf{r}, \mathbf{r}_0) d\mathbf{r}, \quad (13)$$

$$R_{hv}^{(m)}(\mathbf{r}_0) = \int R_{hv}(\mathbf{r})I(\mathbf{r}, \mathbf{r}_0) d\mathbf{r}. \quad (14)$$

In (13) and (14), it is assumed that antenna patterns are identical at the two orthogonal polarizations. The measured differential phase $\Phi_{DP}^{(m)}$ and cross-correlation coefficient $\rho_{hv}^{(m)}$ are

$$\begin{aligned} \Phi_{DP}^{(m)} &= \arg(R_{hv}^{(m)}) \\ \rho_{hv}^{(m)} &= \frac{R_{hv}^{(m)}}{(Z_h^{(m)}Z_v^{(m)})^{1/2}}. \end{aligned} \quad (15)$$

The values of $\Phi_{DP}^{(m)}$ and $\rho_{hv}^{(m)}$ depend on the distributions of $Z_{h,v}^{(e)}$ and R_{hv} within the radar resolution volume and on the shape of antenna pattern. In this study, we assume that a two-way antenna power pattern is axisymmetric and Gaussian (Doviak and Zrnic 1993):

$$I(\theta, \phi) = \frac{1}{2\pi\sigma^2} \exp\left(-\frac{\theta^2 + \phi^2}{2\sigma^2}\right), \quad (16)$$

where θ and φ are elevation and azimuth, respectively, and $\sigma = \Omega/4(\ln 2)^{1/2}$ (Ω is a one-way 3-dB antenna pattern width).

Next we assume that reflectivity factors $Z_{h,v}^{(e)}$ and Z_{hv} expressed in logarithmic scale vary linearly in both cross-beam directions, θ and ϕ :

$$10 \log[Z_{h,v}^{(e)}(\theta, \phi)] = Z_{H,V}^{(e)}(0, 0) + \frac{dZ_{H,V}^{(e)}}{d\theta} \theta + \frac{dZ_{H,V}^{(e)}}{d\phi} \phi, \quad (17)$$

$$10 \log[Z_{hv}(\theta, \phi)] = Z_{HV}(0, 0) + \frac{dZ_{HV}}{d\theta} \theta + \frac{dZ_{HV}}{d\phi} \phi. \quad (18)$$

Similar assumption is made for differential phase Φ_{DP}' :

$$\Phi_{DP}'(\theta, \phi) = \Phi_{DP}'(0, 0) + \frac{d\Phi_{DP}'}{d\theta} \theta + \frac{d\Phi_{DP}'}{d\phi} \phi. \quad (19)$$

Note that, throughout the paper, an uppercase subscript is attributed to radar reflectivity and differential reflectivity in logarithmic scale, whereas lowercase subscript signifies the corresponding variables expressed in the linear scale. Arguments (0, 0) in Eqs. (17)–(19) correspond to the center of the antenna beam.

As a result,

$$Z_{h,v}^{(m)} = Z_{h,v}^{(e)}(0, 0)J_{h,v}^{(\theta)}J_{h,v}^{(\phi)}, \quad (20)$$

$$R_{hv}^{(m)} = Z_{hv}(0, 0)e^{j\Phi_{DP}'(0,0)}J^{(\theta)}J^{(\phi)}, \quad (21)$$

where

$$\begin{aligned} J_{h,v}^{(\theta)} &= \frac{1}{\sqrt{2\pi\sigma}} \int \exp\left(0.23\frac{dZ_{H,V}^{(e)}}{d\theta} \theta - \frac{\theta^2}{2\sigma^2}\right) d\theta \\ &= \exp\left[\frac{(0.23)^2}{2} \sigma^2 \left(\frac{dZ_{H,V}^{(e)}}{d\theta}\right)^2\right], \end{aligned} \quad (22)$$

$$\begin{aligned} J_{h,v}^{(\phi)} &= \frac{1}{\sqrt{2\pi\sigma}} \int \exp\left(0.23\frac{dZ_{H,V}^{(e)}}{d\phi} \phi - \frac{\phi^2}{2\sigma^2}\right) d\phi \\ &= \exp\left[\frac{(0.23)^2}{2} \sigma^2 \left(\frac{dZ_{H,V}^{(e)}}{d\phi}\right)^2\right], \end{aligned} \quad (23)$$

$$\begin{aligned} J^{(\theta)} &= \frac{1}{\sqrt{2\pi\sigma}} \int \exp\left(j\frac{d\Phi_{DP}'}{d\theta} \theta + 0.23\frac{dZ_{HV}}{d\theta} \theta - \frac{\theta^2}{2\sigma^2}\right) d\theta \\ &= \exp\left[\frac{\sigma^2}{2} \left(j\frac{d\Phi_{DP}'}{d\theta} + 0.23\frac{dZ_{HV}}{d\theta}\right)^2\right], \end{aligned} \quad (24)$$

$$\begin{aligned} J^{(\phi)} &= \frac{1}{\sqrt{2\pi\sigma}} \int \exp\left(j\frac{d\Phi_{DP}'}{d\phi} \phi + 0.23\frac{dZ_{HV}}{d\phi} \phi - \frac{\phi^2}{2\sigma^2}\right) d\phi \\ &= \exp\left[\frac{\sigma^2}{2} \left(j\frac{d\Phi_{DP}'}{d\phi} + 0.23\frac{dZ_{HV}}{d\phi}\right)^2\right]. \end{aligned} \quad (25)$$

The measured differential reflectivity is expressed as

$$Z_{dr}^{(m)} = Z_{dr}^{(e)}(0, 0) \frac{J_h^{(\theta)}J_v^{(\phi)}}{J_v^{(\theta)}J_h^{(\phi)}} = Z_{dr}^{(e)}(0, 0) \exp\left\{\frac{(0.23)^2}{2} \sigma^2 \left[\left(\frac{dZ_H^{(e)}}{d\theta}\right)^2 - \left(\frac{dZ_V^{(e)}}{d\theta}\right)^2 + \left(\frac{dZ_H^{(e)}}{d\phi}\right)^2 - \left(\frac{dZ_V^{(e)}}{d\phi}\right)^2\right]\right\}. \quad (26)$$

Since

$$Z_H^{(e)} - Z_V^{(e)} = Z_{DR}^{(e)} \quad \text{and} \quad 2 \frac{dZ_H^{(e)}}{d\theta} \gg \frac{dZ_{DR}^{(e)}}{d\theta}, \quad 2 \frac{dZ_H^{(e)}}{d\phi} \gg \frac{dZ_{DR}^{(e)}}{d\phi}, \quad (27)$$

we can further simplify

$$Z_{dr}^{(m)} \approx Z_{dr}^{(e)} \exp \left\{ (0.23)^2 \sigma^2 \left[\frac{dZ_H^{(e)}}{d\theta} \frac{dZ_{DR}^{(e)}}{d\theta} + \frac{dZ_H^{(e)}}{d\phi} \frac{dZ_{DR}^{(e)}}{d\phi} \right] \right\}. \quad (28)$$

Or, equivalently,

$$Z_{DR}^{(m)} \approx Z_{DR}^{(e)} + 0.23 \sigma^2 \left[\frac{dZ_H^{(e)}}{d\theta} \frac{dZ_{DR}^{(e)}}{d\theta} + \frac{dZ_H^{(e)}}{d\phi} \frac{dZ_{DR}^{(e)}}{d\phi} \right]. \quad (29)$$

The measured differential phase can be written as

$$\xi_2 = \exp \left(\frac{(0.23)^2}{2} \sigma^2 \left\{ \left(\frac{dZ_{HV}^{(e)}}{d\theta} \right)^2 + \left(\frac{dZ_{HV}^{(e)}}{d\phi} \right)^2 - \frac{1}{2} \left[\left(\frac{dZ_H^{(e)}}{d\theta} \right)^2 + \left(\frac{dZ_H^{(e)}}{d\phi} \right)^2 + \left(\frac{dZ_V^{(e)}}{d\theta} \right)^2 + \left(\frac{dZ_V^{(e)}}{d\phi} \right)^2 \right] \right\} \right). \quad (34)$$

If $|\rho_{hv}| \approx 1$, then

$$\xi_2 \approx \exp \left\{ -\frac{(0.23)^2}{8} \sigma^2 \left[\left(\frac{dZ_{DR}^{(e)}}{d\theta} \right)^2 + \left(\frac{dZ_{DR}^{(e)}}{d\phi} \right)^2 \right] \right\}. \quad (35)$$

The coefficient ξ_2 is usually very close to 1, hence we will ignore this term in our further considerations.

Expressing the parameter σ via the antenna beamwidth Ω , we finally arrive at the following approximate

$$\frac{|\rho_{hv}^{(m)}|}{|\rho_{hv}|} = \xi_1 = \exp \left\{ -1.37 \times 10^{-5} \Omega^2 \left[\left(\frac{d\Phi'_{DP}}{d\theta} \right)^2 + \left(\frac{d\Phi'_{DP}}{d\phi} \right)^2 \right] \right\}. \quad (38)$$

In Eqs. (36)–(38), Φ'_{DP} , $\Delta\Phi_{DP}$, Ω , θ , and ϕ are expressed in degrees, whereas Z_H , Z_{HV} , ΔZ_{DR} , and Z_{DR} are in decibels.

Similar formulas can be obtained for the NBF-related bias of the radar reflectivity factor at horizontal polarization:

$$\Delta Z_H(dB) \approx 0.01 \Omega^2 \left[\left(\frac{dZ_H^{(e)}}{d\theta} \right)^2 + \left(\frac{dZ_H^{(e)}}{d\phi} \right)^2 \right]. \quad (39)$$

$$\Phi_{DP}^{(m)} = \arg(R_{hv}^{(m)}) = \Phi'_{DP}(0, 0) + \Delta\Phi_{DP}, \quad (30)$$

where

$$\Delta\Phi_{DP} = 0.23 \sigma^2 \left(\frac{d\Phi'_{DP}}{d\theta} \frac{dZ_{HV}}{d\theta} + \frac{d\Phi'_{DP}}{d\phi} \frac{dZ_{HV}}{d\phi} \right). \quad (31)$$

Similarly, the magnitude of the measured cross-correlation coefficient is expressed as

$$|\rho_{hv}^{(m)}| = \frac{Z_{hv}(0, 0)}{[Z_h^{(e)}(0, 0)Z_v^{(e)}(0, 0)]^{1/2}} \frac{|J^{(\theta)} J^{(\phi)}|}{[J_h^{(\theta)} J_v^{(\theta)} J_h^{(\phi)} J_v^{(\phi)}]^{1/2}} \\ = |\rho_{hv}(0, 0)| \xi_1 \xi_2, \quad (32)$$

where

$$\xi_1 = \exp \left\{ -\frac{\sigma^2}{2} \left[\left(\frac{d\Phi'_{DP}}{d\theta} \right)^2 + \left(\frac{d\Phi'_{DP}}{d\phi} \right)^2 \right] \right\} \quad (33)$$

formulas for the biases of Z_{DR} , Φ_{DP} , and ρ_{hv} that will be used in the subsequent analysis in the paper:

$$\Delta Z_{DR} = 0.02 \Omega^2 \left(\frac{dZ_H^{(e)}}{d\theta} \frac{dZ_{DR}^{(e)}}{d\theta} + \frac{dZ_H^{(e)}}{d\phi} \frac{dZ_{DR}^{(e)}}{d\phi} \right), \quad (36)$$

$$\Delta\Phi_{DP} = 0.02 \Omega^2 \left(\frac{d\Phi'_{DP}}{d\theta} \frac{dZ_{HV}^{(e)}}{d\theta} + \frac{d\Phi'_{DP}}{d\phi} \frac{dZ_{HV}^{(e)}}{d\phi} \right), \quad (37)$$

As expected, the NBF-induced bias of Z is always positive if reflectivity varies linearly in both orthogonal directions within the radar resolution volume. It follows from Eq. (39) that for a 1° beam the corresponding Z bias exceeds 1 dB if the gradient of Z is higher than 10 dB deg^{-1} in any of the two transverse directions. We will not address ΔZ_H anymore in the paper since the focus of this study is on the impact of beam broadening on the quality of polarimetric variables.

3. NBF effects in the case of the mesoscale convective system

The gradients of Z_H , Z_{HV} , Z_{DR} , and Φ_{DP} in Eqs. (36)–(38) can be approximately estimated from real data by comparing the corresponding variables at adjacent radials. We perform such estimation in the case of a mesoscale convective system (MCS) that was observed with the polarimetric prototype of the S-band WSR-88D radar (hereafter KOUN) in central Oklahoma on 2 June 2004. The analysis was conducted using the data from two lowest plan position indicators (PPIs) at elevations of 0.44° and 1.45° . Horizontal gradients were computed from the data collected at the lowest elevation, whereas vertical gradients were estimated using the data at both elevations.

Strictly speaking, such a procedure underestimates the magnitude of intrinsic gradients because the data are smeared with the antenna beam. Indeed, the transverse dimension of the radar resolution volume exceeds 3 km at 200 km from the radar if the antenna beamwidth is 1° . Hence, smaller-scale cross-beam nonuniformities of the precipitation field are not resolved. Nevertheless, as will be shown later, these approximate estimates of gradients prove to be very useful for evaluating the quality of polarimetric data.

A composite plot of Z_H , Z_{DR} , Φ_{DP} , and ρ_{hv} at elevation 0.44° (Fig. 1) corresponds to the time when an extensive squall line passes over the radar and produces tremendous attenuation and differential attenuation that are clearly visible in the eastern sector. The radar reflectivity factor and differential reflectivity are deliberately not corrected for attenuation in order to estimate the gradients of $Z_H^{(e)}$, $Z_{HV}^{(e)}$, and $Z_{DR}^{(e)}$, which are affected by attenuation according to their definition in (7)–(11). High values of Φ_{DP} in the eastern sector are accompanied by negatively biased Z and Z_{DR} and a pronounced drop in the cross-correlation coefficient ρ_{hv} . While the drop in Z_{DR} well below -2 dB is caused by differential attenuation, the decrease in ρ_{hv} is a result of NBF.

This is confirmed by Fig. 2 where the fields of the parameters ΔZ_{DR} , $\Delta\Phi_{DP}$, and ξ computed from Eqs. (36)–(38) are displayed together with Z_H . The ρ_{hv} depression in Fig. 2d is very well correlated with the observed decrease of the measured ρ_{hv} in Fig. 1. The magnitude of the negative ρ_{hv} bias exceeds 0.2. Such a strong bias adversely affects the quality of the polarimetric classification of radar echoes and induces large statistical errors in the estimates of all polarimetric variables. Similar radial features or “valleys” of lower ρ_{hv} are frequently observed in the KOUN polarimetric data. Their primary cause is large vertical gradient of

Φ_{DP} . The ray at a higher elevation overshoots precipitation at closer distances from the radar than the ray at lower tilt. Therefore, the differential phase at higher tilt stops increasing earlier (i.e., at closer slant ranges) than the one at lower tilt. While both higher and lower rays are still in rain, the differential phases at the two rays grow proportionally and the difference between them is not high. However, once the higher ray intercepts the freezing level, the corresponding Φ_{DP} stops increasing, whereas Φ_{DP} at the lower ray continues its growth. This explains a radial character of the observed artifacts and their severity, which progresses with range.

According to (38), large gradients of Φ_{DP} are responsible for the decrease in ρ_{hv} . In contrast, perturbations of Φ_{DP} are determined by both the gradients of the differential phase and the reflectivity factor. As a result, $\Delta\Phi_{DP}$ exhibits more complex and nonmonotonic behavior along the radial than the factor ξ . If the reflectivity field is relatively uniform as in the stratiform region of the MCS north-northeast of the squall line, then the gradients of Φ_{DP} dominate and apparent radial features are evident in the field of $\Delta\Phi_{DP}$.

The NBF-related bias in differential reflectivity can also be significant and may exceed several tenths of a decibel as Fig. 2b shows. Positive biases of Z_{DR} are common in convective areas of the storm not far away from the radar, whereas negative biases are prevalent at longer distances in convective and stratiform parts of the MCS. The latter feature is explained by the general decrease of Z_{DR} with height. The Z_{DR} biases, as well as the biases in Φ_{DP} and ρ_{hv} , tend to increase with range as a result of beam broadening.

A similar analysis was performed on the data collected for the same storm but 2 h after the squall line passed over the radar and was viewed at a different angle (Figs. 3 and 4). At that moment, attenuation effects were much weaker and the differential phase was significantly lower. Again, the area of ρ_{hv} depression is well predicted from the analysis of gradients. The perturbations of the Φ_{DP} radial profiles are also in good agreement with their estimates from the gradients in accordance with Eq. (37).

In Fig. 5, measured range dependencies of Φ_{DP} (thin curves) are compared with radial profiles of $\Delta\Phi_{DP}$ calculated from (37) (thick curves) for six successive azimuths belonging to the sector indicated in Fig. 4d. Despite many simplified assumptions made in the evaluation of $\Delta\Phi_{DP}$, the correlation between the Φ_{DP} and $\Delta\Phi_{DP}$ profiles is surprisingly high. The most pronounced excursions of the Φ_{DP} curves, such as spikes and depressions, are well reproduced in the modeled $\Delta\Phi_{DP}$. Thus, they are primarily attributed to NBF rather than pure statistical errors in Φ_{DP} estimation or

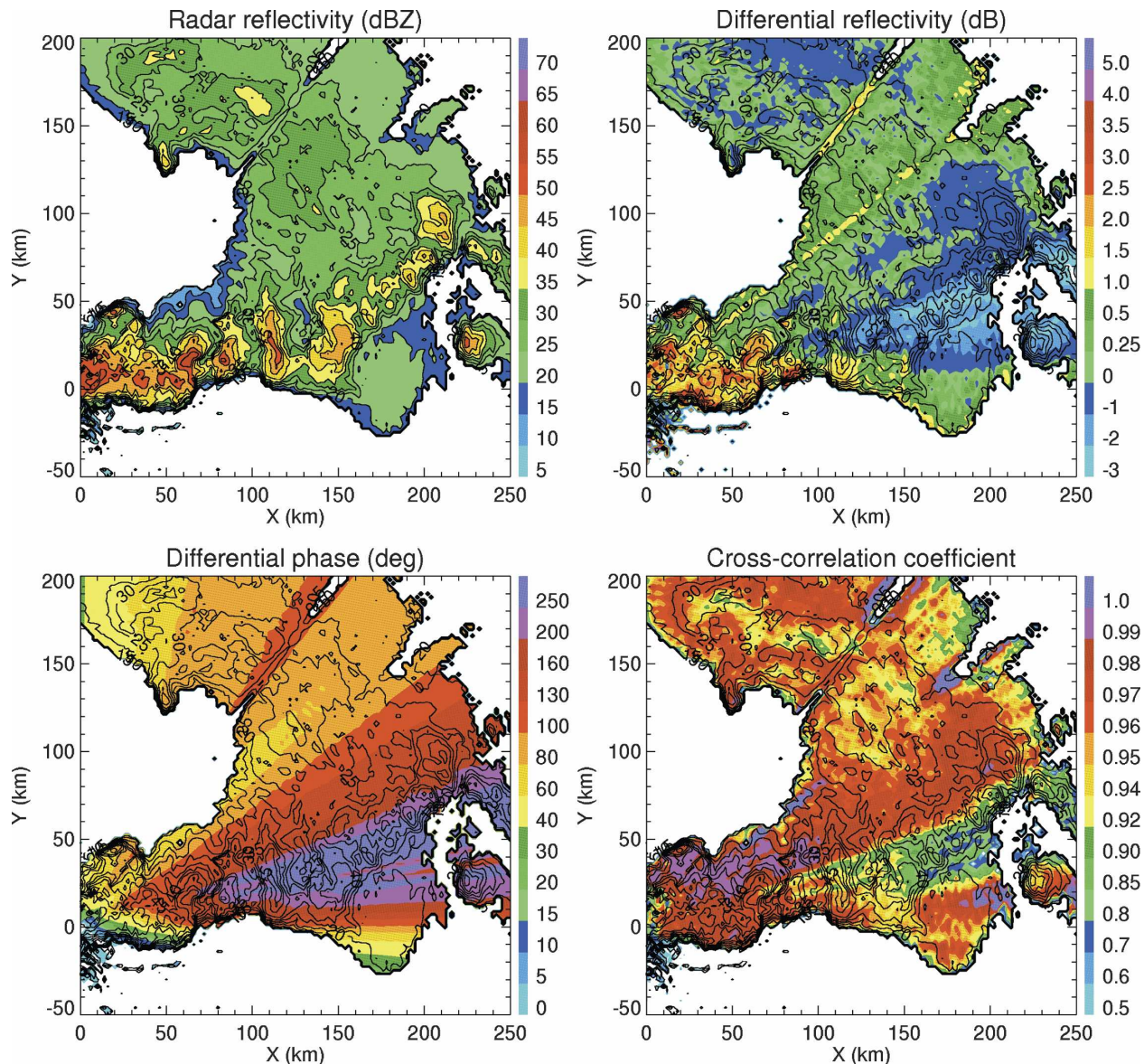


FIG. 1. Composite plot of Z , Z_{DR} , Φ_{DP} , and ρ_{hv} measured by the KOUN WSR-88D radar at 2038 UTC 2 Jun 2004. Elevation is 0.44° . Overlaid are contours of Z . No correction for attenuation has been made. The data are displayed for $SNR > 5$ dB.

to the contribution from the backscatter differential phase.

4. Beam-broadening effects in the case of stratiform rain

The melting layer or bright band is a special case of strong vertical nonuniformity in stratiform precipitation. The bright band is associated with very well pronounced polarimetric signatures such as the sharp Z_{DR} maximum and ρ_{hv} minimum. These signatures have very important prognostic value because the top of the

melting layer corresponds to the freezing level and its bottom represents the boundary between pure liquid and mixed-phase hydrometeors. The latter one marks the onset of the brightband contamination in radar rainfall estimates. Accurate designation of the melting layer is a key for successful discrimination between liquid and frozen hydrometeors (Giangrande et al. 2005).

Because the thickness of the bright band is only few hundreds of meters, the corresponding polarimetric signatures degrade very rapidly with range even for the radar beam as narrow as 1° . This degradation is illustrated in the range–height indicator (RHI) plot of Z ,

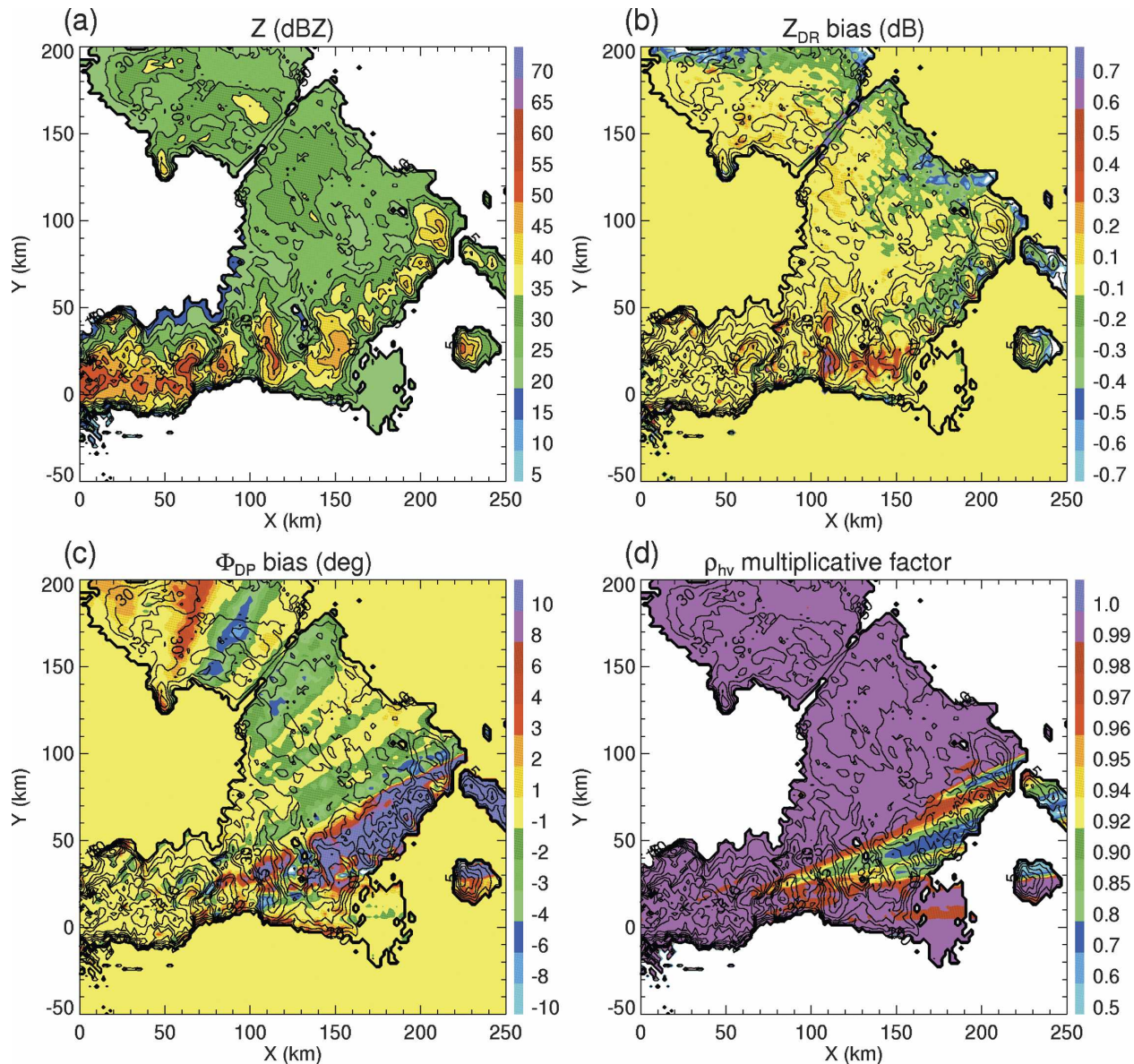


FIG. 2. Composite plot of (a) Z , (b) ΔZ_{DR} , (c) $\Delta\Phi_{DP}$, and (d) ξ (multiplicative factor of ρ_{hv}) corresponding to PPI in Fig. 1. The biases of Z_{DR} , Φ_{DP} , and ρ_{hv} are attributed to NBF and computed from Eqs. (36)–(38). Overlaid are contours of Z . The data are displayed for $SNR > 10$ dB.

Z_{DR} , Φ_{DP} , and ρ_{hv} measured with the KOUN radar on 7 April 2002 (Fig. 6). To quantify the degree of such deterioration at longer distances from the radar one has to use a more sophisticated model of NBF than is described in section 2.

For the case illustrated in Fig. 6, we obtained average vertical profiles of all radar variables at very close distances from the radar and modeled the RHI fields of Z , Z_{DR} , Φ_{DP} , and ρ_{hv} at the S band for different antenna beamwidths assuming the horizontal homogeneity of the intrinsic fields of these radar variables. The results

of such modeling studies are presented in Figs. 7 and 8 for antenna beamwidths at 1° and 2° . Modeled fields in Fig. 7 are very consistent with what was actually observed with the same antenna beamwidth (Fig. 6). This means that the model adequately reproduces observational data.

A twofold increase of the radar beamwidth leads to the enhanced brightband contamination of the low-altitude echoes in rain (Fig. 8). At the lowest elevations, the differential reflectivity and cross-correlation coefficients quickly acquire the values typical for melting hy-

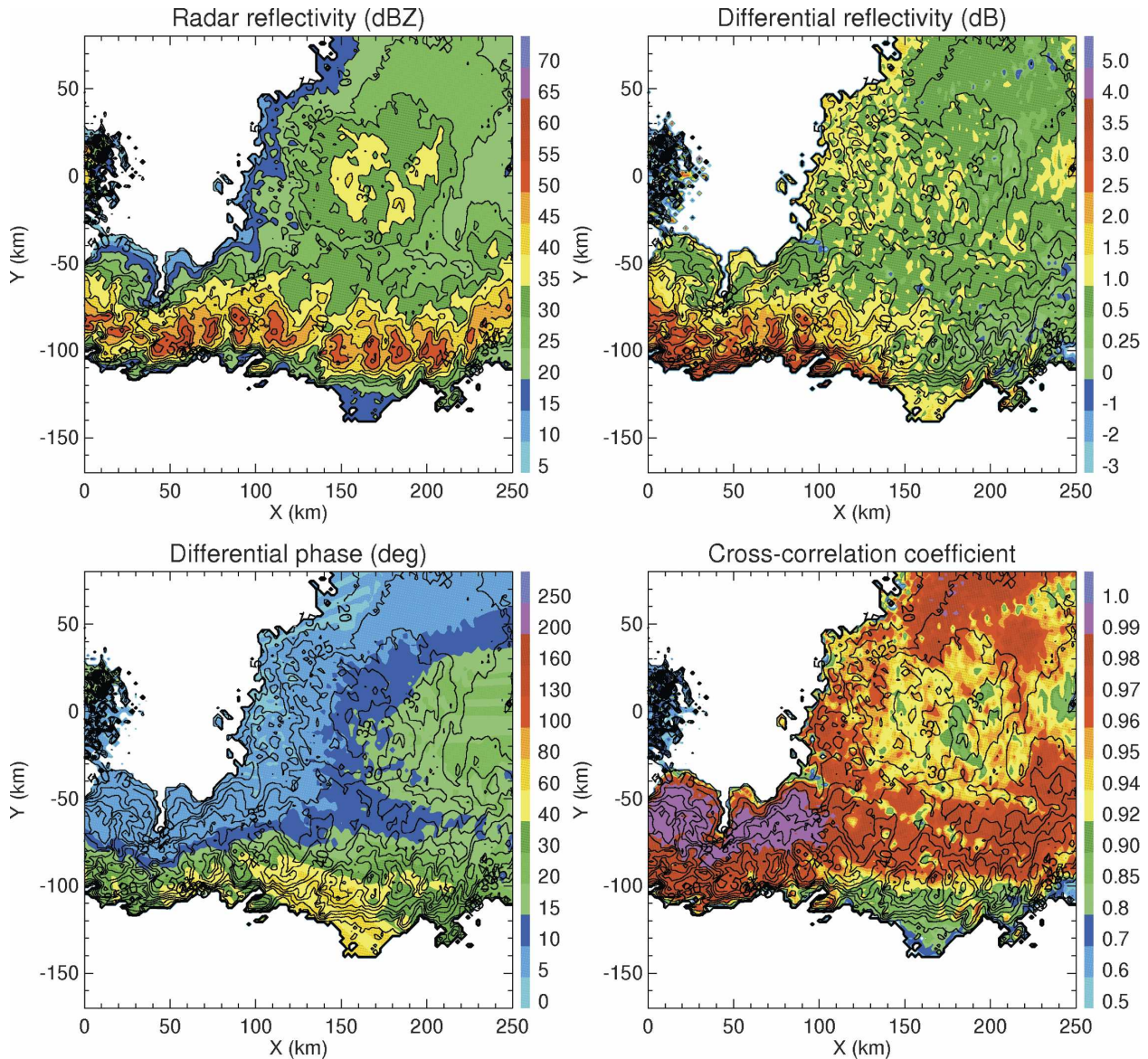


FIG. 3. Composite plot of Z , Z_{DR} , Φ_{DP} , and ρ_{hv} measured by the KOUN WSR-88D radar at 2231 UTC 2 Jun 2004. Elevation is 0.44° . Overlaid are contours of Z . No correction for attenuation has been made. The data are displayed for $SNR > 5$ dB.

drometeors. As in the case of the MCS, vertical non-uniformity causes wavelike perturbation of the Φ_{DP} profile in the melting layer as was explained by Ryzhkov and Zrnic (1998). Below the melting layer, the mean value of Φ_{DP} is less biased but differential phase becomes more noisy due to lowering of ρ_{hv} at the altitudes below the physical (i.e., intrinsic) bottom of the bright band.

5. Discussion

The findings in this study may have important practical implications to all users of polarimetric radar data.

This is significant in view of the forthcoming polarimetric upgrade of the U.S. National Weather Service network of the WSR-88D radars. One should avoid using polarimetric variables in a quantitative manner in the areas where these variables are significantly affected by NBF. Such areas can be identified by computing horizontal and vertical gradients of the radar reflectivity, the differential reflectivity, and the differential phase as well as estimating the biases of Z_{DR} , Φ_{DP} , and ρ_{hv} according to Eqs. (36)–(38). The procedure for gradient estimation is simple and straightforward.

If the magnitudes of ΔZ_{DR} , $\Delta \Phi_{DP}$, and the difference

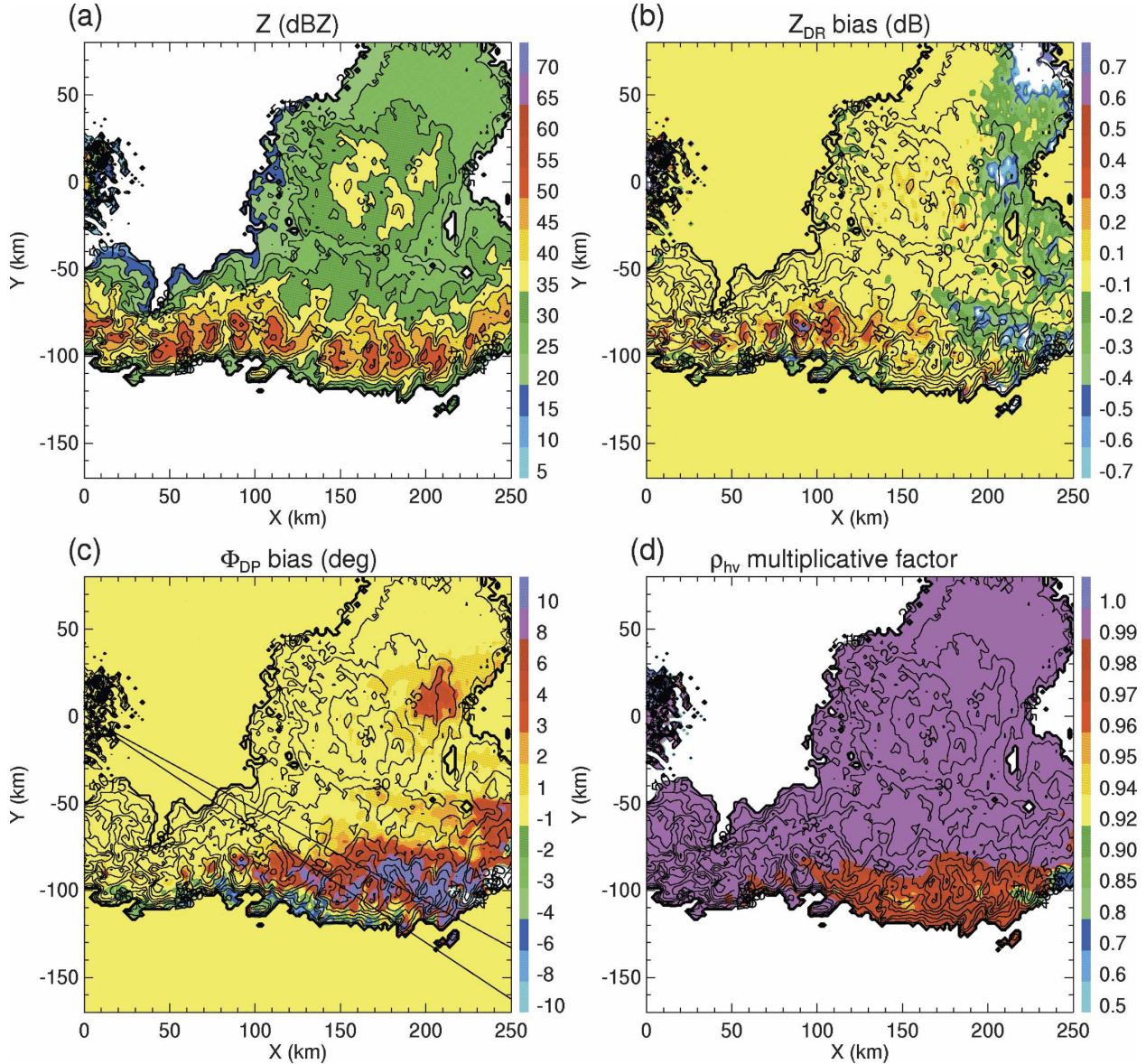


FIG. 4. Composite plot of (a) Z , (b) ΔZ_{DR} , (c) $\Delta\Phi_{DP}$, and (d) ξ (multiplicative factor of ρ_{hv}) corresponding to PPI in Fig. 3. The biases of Z_{DR} , Φ_{DP} , and ρ_{hv} are attributed to NBF and computed from Eqs. (36)–(38). Overlaid are contours of Z . The data are displayed for $SNR > 10$ dB.

$1 - \xi$ exceed certain thresholds, then the corresponding variables (Z_{DR} , K_{DP} , and ρ_{hv}) should not be used for estimating polarimetric products in these areas. The choice of such thresholds is dictated by tolerable errors that depend on particular applications. For example, the Z_{DR} bias has to be less than 0.2 dB if Z_{DR} is utilized for rainfall estimation. The biases of Φ_{DP} within $\pm 2^\circ$ are acceptable because the statistical fluctuations of the Φ_{DP} estimate are between 1° and 2° for typical dwell times used for operational weather radars. The bias of 0.02 in ρ_{hv} may also be tolerable for classification purposes.

In addition to the negative impact on the quality of polarimetric classification, the decrease of ρ_{hv} is detrimental for statistical accuracy of the estimates of Z_{DR} , Φ_{DP} , and ρ_{hv} itself. Indeed, the standard deviations of the estimates for all three variables are proportional to $(1 - \rho_{hv}^2)^{1/2}$ (Bringi and Chandrasekar 2001). This means that if ρ_{hv} drops from 0.99 to 0.90, the corresponding errors increase 3 times.

Perturbations of the Φ_{DP} radial profile produce erroneous estimates of K_{DP} of both signs. Although negative K_{DP} s are easily identified (and sometimes taken out as unphysical), positively biased K_{DP} s usually go

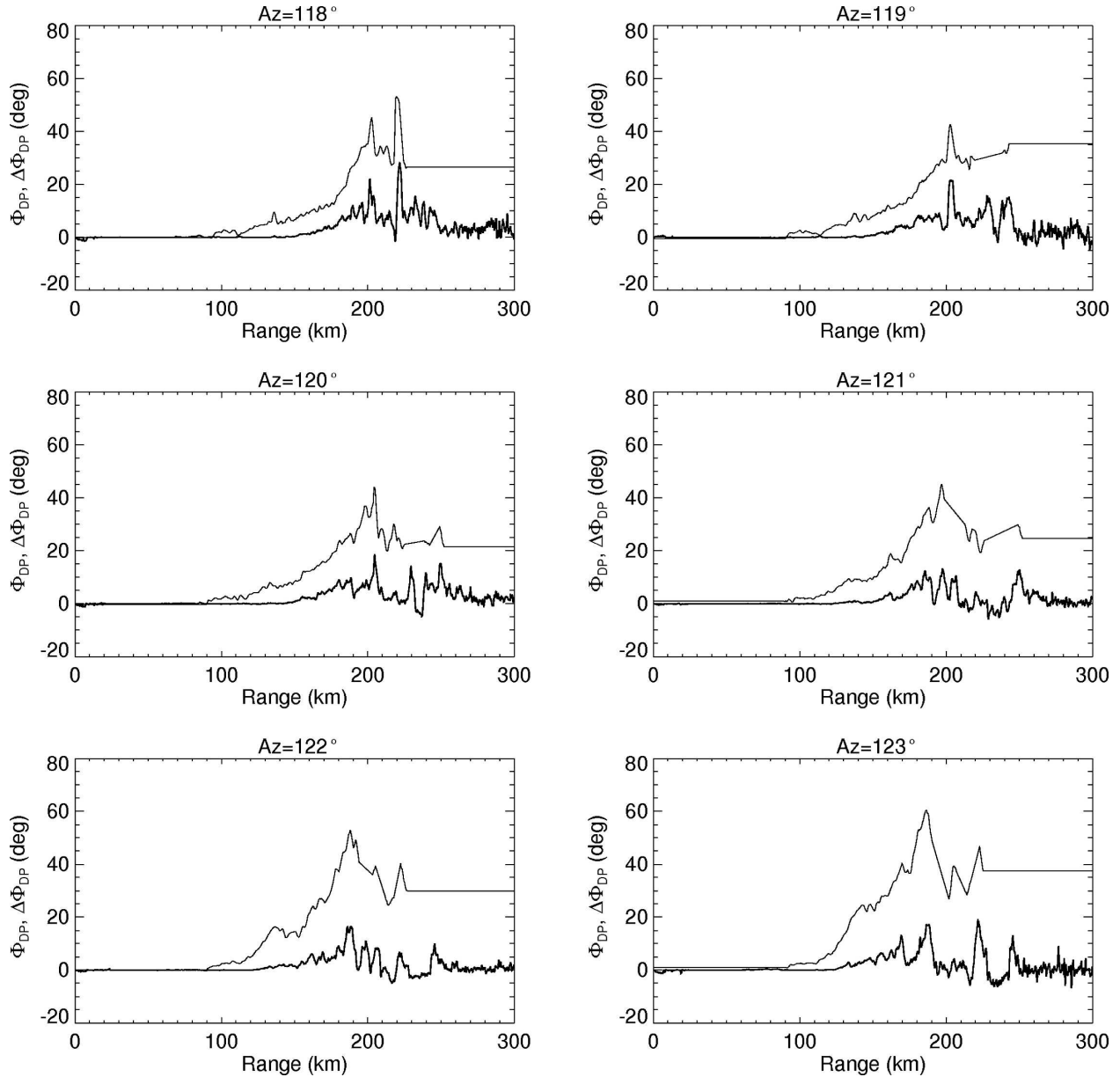


FIG. 5. Radial profiles of Φ_{DP} (thin curves) and its bias ($\Delta\Phi_{DP}$, thick curves) caused by NBF at six adjacent azimuths within the sector shown in Fig. 4c. The antenna elevation is 0.44° .

undetected. Since K_{DP} is a slope of the Φ_{DP} radial profile, the bias in K_{DP} is not necessarily zero if $\Delta\Phi_{DP} = 0$. Thus, the data with $\Delta\Phi_{DP} = 0$ in the vicinity of large $|\Delta\Phi_{DP}|$ should be also scrutinized.

The magnitudes of ΔZ_{DR} , $\Delta\Phi_{DP}$, and $1 - \xi$ depend on the square of antenna beamwidth. Such a strong dependence may preclude the use of wide-beam antennas for polarimetric measurements. A twofold increase of the beamwidth from 1° to 2° leads to 4-times-larger biases and significant deterioration of the melting layer designation as Figs. 7 and 8 show.

The biases of Φ_{DP} and ρ_{hv} are wavelength dependent because the differential phase and its gradients are inversely proportional to the radar wavelength λ . The impact on $\Delta\Phi_{DP}$ is proportional to λ^{-1} , whereas the ρ_{hv} bias is approximately proportional to λ^{-2} . Enhanced attenuation and differential attenuation at shorter wavelengths may either increase or decrease the gradients of Z and Z_{DR} . In some situations, these changes in the Z and Z_{DR} gradients may offset the increase in the gradient of Φ_{DP} and its greater impact on the NBF-related biases in Φ_{DP} and ρ_{hv} . However, cursory analy-

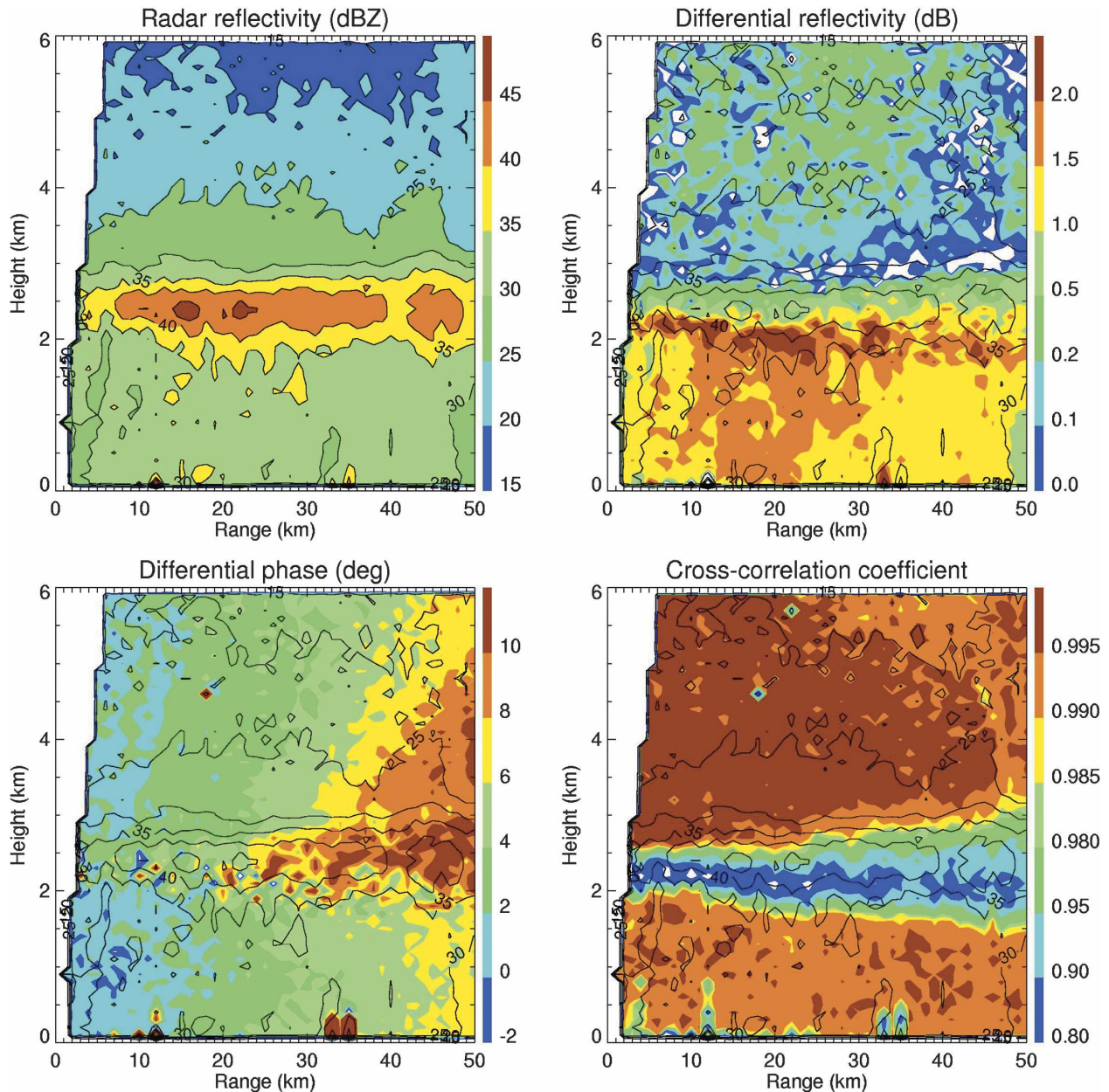


FIG. 6. Composite RHI plot of Z , Z_{DR} , Φ_{DP} , and ρ_{hv} measured with the KOUN WSR-88D radar on 7 Apr 2002.

sis of the C- and X-band-simulated and observed polarimetric data reveals stronger NBF effects compared to the S band (Ryzhkov and Zrníc 2005). Although range coverage of the shorter-wavelength radars is usually smaller than the one for S-band weather radars and the antenna beam is not as broad at closer distances, all mentioned problems should be taken seriously. In convective situations, both attenuation and beamwidth effects may restrict the use of polarimetric methods on short-wavelength radars (particularly with antenna beams wider than 1°).

We emphasize that Eqs. (36)–(38) cannot be used for *correction* of Z_{DR} , Φ_{DP} , and ρ_{hv} because the bias estimates are very approximate due to many simplifying assumptions made in derivation of these equations. Instead, we recommend using ΔZ_{DR} , $\Delta \Phi_{DP}$, and ξ as *quality indexes* for the corresponding radar variables. Such an approach is used in the algorithms for hydrometeor classification and rainfall estimation developed at the National Severe Storms Laboratory (NSSL) for operational utilization with the polarimetric prototype of the WSR-88D radar. According to this approach, each ra-

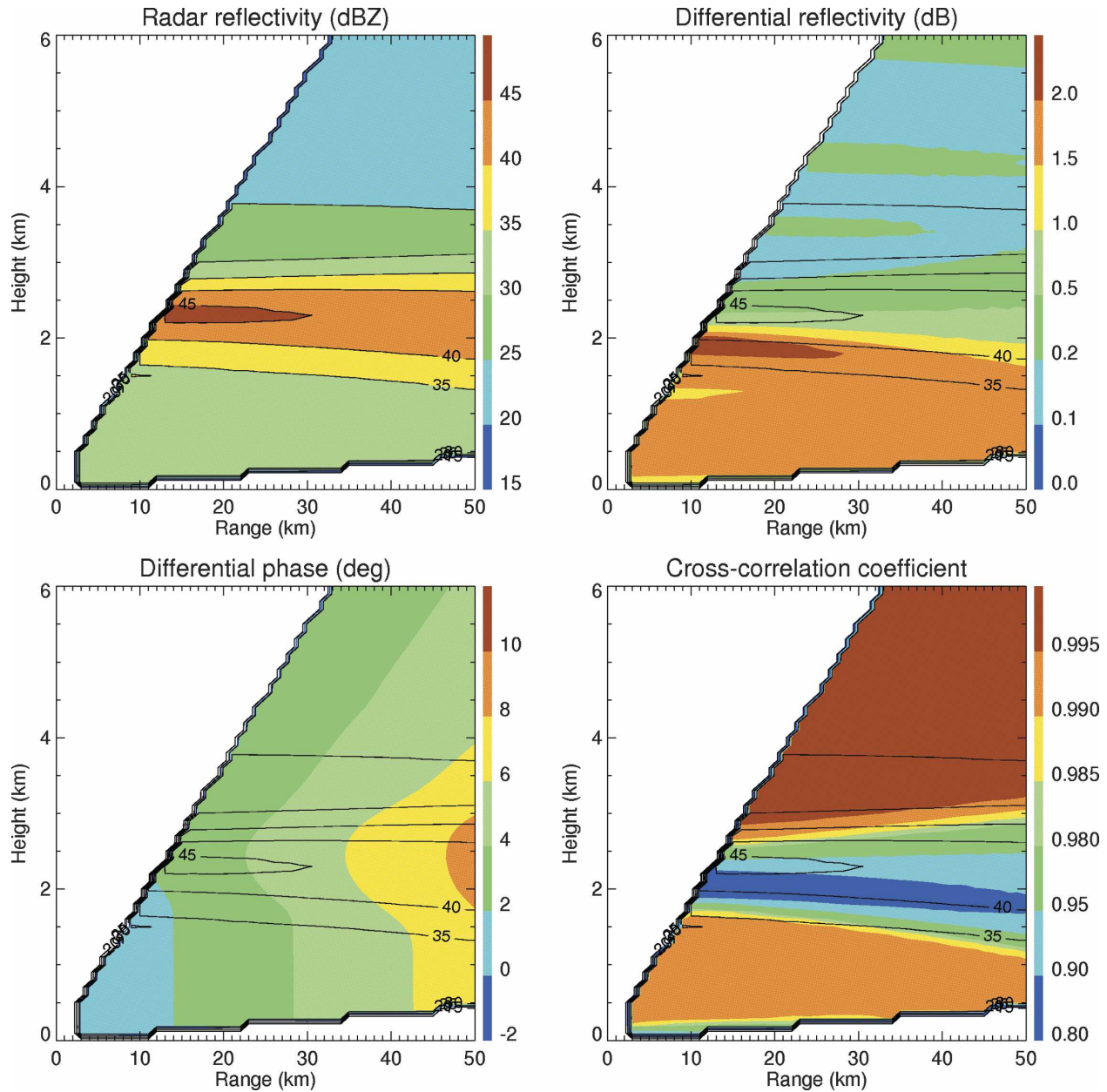


FIG. 7. Composite RHI plot of simulated Z , Z_{DR} , Φ_{DP} , and ρ_{hv} for the beamwidth of 1° . Intrinsic vertical profiles of radar variables were obtained from averaging the measured data at close distances from the radar (Fig. 6). Horizontal uniformity is assumed.

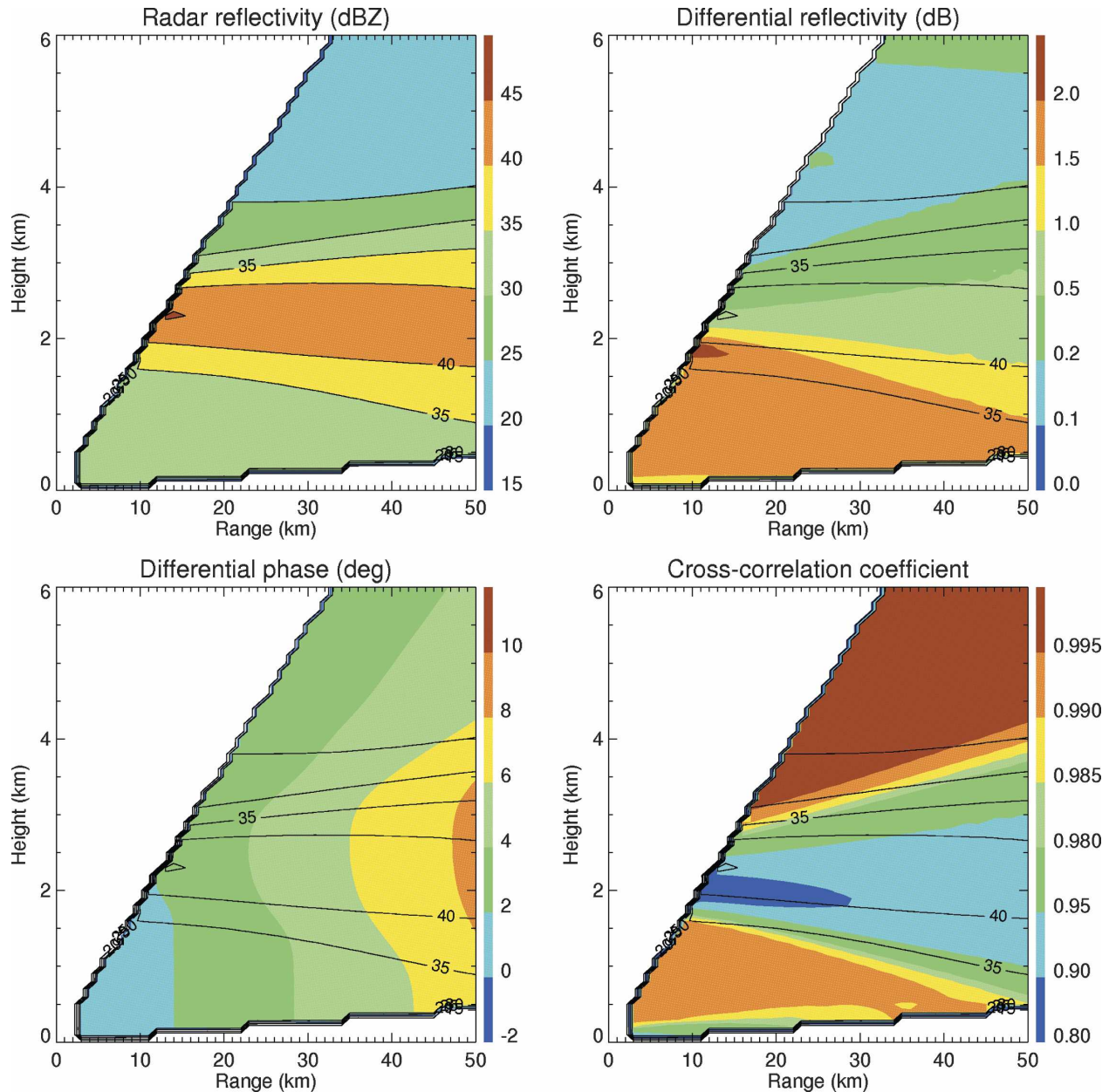
dar variable is supplemented with its confidence factor that may depend on ΔZ_{DR} , $\Delta \Phi_{DP}$, and ξ along with a signal-to-noise ratio, the total differential phase (which characterizes potential impact of attenuation/differential attenuation), the magnitude of ρ_{hv} (which characterizes the noisiness of polarimetric data), etc.

6. Conclusions

In this study, we evaluate the impact of nonuniform beam filling (NBF) on the quality of polarimetric mea-

surements. It is shown that such an impact can be quite significant, especially at longer distances from the radar due to progressive broadening of the antenna beam.

Relatively simple analytical formulas have been obtained for the NBF-induced biases of the differential reflectivity Z_{DR} , the differential phase Φ_{DP} , and the cross-correlation coefficient ρ_{hv} assuming linear gradients of radar reflectivity Z_H , Z_{DR} , and Φ_{DP} in the cross-beam directions within the radar resolution volume. It is found that the biases are proportional to the square

FIG. 8. Same as in Fig. 7, but for the beamwidth of 2° .

of the antenna beamwidth. The bias of Z_{DR} does not depend on the radar wavelength, whereas the biases of Φ_{DP} and ρ_{hv} increase at shorter wavelength (proportionally to λ^{-1} in the case of Φ_{DP} and to λ^{-2} in the case of ρ_{hv}). Thus, the NBF effects are stronger at C and X bands than at the S band.

Horizontal and vertical gradients of Z_H , Z_{DR} , and Φ_{DP} were estimated from polarimetric data collected by the S-band KOUN WSR-88D radar in a mesoscale convective system. Joint analysis of the measured fields of polarimetric variables and their NBF-induced biases

computed from the cross-beam gradients proves that nonuniform beam filling combined with beam broadening is responsible for such commonly observed artifacts as radial “valleys” of ρ_{hv} depression and oscillatory behavior of the Φ_{DP} profiles. The latter usually manifests itself as the appearance of negative K_{DP} . It is also shown that polarimetric signatures of the melting layer rapidly degrade with distance as the antenna beam widens.

Although correcting Z_{DR} , Φ_{DP} , and ρ_{hv} for such biases is not practical because the biases cannot be esti-

mated with sufficient accuracy, their approximate estimates are important as “quality indexes” of the corresponding polarimetric variables. One should abstain from any quantitative use of the variable if the respective NBF-caused bias exceeds the threshold of acceptability.

These considerations should be taken into account in using polarimetric data at different wavelengths and various angular resolutions and in developing robust algorithms for polarimetric hydrometeor classification and rainfall estimation.

Acknowledgments. Funding for this study was provided by NOAA/Office of Oceanic and Atmospheric Research under NOAA/University of Oklahoma Cooperative Agreement NA17RJ1227, the U.S. Department of Commerce, and from the U.S. National Weather Service, the Federal Aviation Administration (FAA), and the Air Force Weather Agency through the NEXRAD Products Improvement Program. I am grateful to Dr. D. Zrníc for reading this manuscript and for making useful comments. The support from the NSSL and the CIMMS, University of Oklahoma staff who maintain and operate the KOUN WSR-88D polarimetric radar is also acknowledged.

APPENDIX

Equations for the Covariance R_{hv}

The voltage vectors of the transmitted (\mathbf{V}^t) and received (\mathbf{V}) waves in the case of individual scatterer are related as (Bringi and Chandrasekar 2001)

$$\begin{pmatrix} V_h \\ V_v \end{pmatrix} = C_1 \begin{pmatrix} T_{hh} & 0 \\ 0 & T_{vv} \end{pmatrix} \begin{pmatrix} s_{hh} & s_{hv} \\ s_{hv} & s_{vv} \end{pmatrix} \begin{pmatrix} T_{hh} & 0 \\ 0 & T_{vv} \end{pmatrix} \begin{pmatrix} V_h^t \\ V_v^t \end{pmatrix}, \quad (\text{A1})$$

where matrix elements s_{hh} , s_{vv} , and s_{hv} represent back-scattering coefficients of the scatterer, and T_{hh} and T_{vv} describe phase shifts and attenuations for H and V waves along propagation path:

$$T_{hh,vv} = \exp(-j\Phi_{h,v} - \Gamma_{h,v}), \quad (\text{A2})$$

where $\Phi_{h,v}$ is the phase shift, $\Gamma_{h,v}$ is the attenuation, and $\Phi_{DP} = 2(\Phi_h - \Phi_v)$ is a differential phase. The coefficient C_1 is defined as

$$C_1 = \frac{G\lambda f^2}{4\pi R^2}. \quad (\text{A3})$$

In (A3), G is the antenna gain, λ is the radar wavelength, R is the distance between the radar and scatterer, and f^2 is the normalized one-way antenna power pattern. It is assumed that the antenna patterns for orthogonal polarizations are the same.

In the case of many scatterers filling the radar resolution volume, the basic Eq. (A1) can be rewritten as

$$\begin{aligned} V_h &= \frac{P_t^{1/2} G \lambda}{4\pi} \sum_i h_i e^{-j2\Phi_h^{(i)}} \\ V_v &= \frac{P_t^{1/2} G \lambda}{4\pi} \sum_i v_i e^{-j2\Phi_v^{(i)}}, \end{aligned} \quad (\text{A4})$$

where $P_t = |V^t|^2$ [$\mathbf{V}^t = (V_h^t, V_v^t)$] and

$$\begin{aligned} h_i &= s_{hh}^{(i)} e^{-2\Gamma_h^{(i)}} f_i^2 / R_i^2 \\ v_i &= s_{vv}^{(i)} e^{-2\Gamma_v^{(i)}} f_i^2 / R_i^2. \end{aligned} \quad (\text{A5})$$

Index i in (A4) and (A5) stands for a number of scatterer. In our derivation we neglect the cross-coupling terms proportional to $s_{hv}^{(i)}$.

The measured covariance $R_{hv}^{(m)}$ is defined as

$$R_{hv}^{(m)} = C_2 \overline{V_h^* V_v}, \quad (\text{A6})$$

where

$$C_2 = \frac{2^{10} \ln 2 \lambda^2 R_0^2}{\pi^3 P_t G^2 c \tau \Omega^2 |K_w|^2}. \quad (\text{A7})$$

The overbar in (A6) means averaging in time. In (A7), R_0 is the distance to the center of the radar resolution volume; c is the speed of light; τ is the radar pulse duration; Ω is the one-way 3-dB antenna pattern width, $K_w = (\epsilon_w - 1) / (\epsilon_w + 2)$, where ϵ_w is the dielectric constant of water. Substituting (A4) into (A6), we obtain

$$R_{hv}^{(m)} = C_3 \left[\sum_i h_i^* v_i e^{j2(\Phi_h^{(i)} - \Phi_v^{(i)})} + \sum_{m \neq n} h_m^* v_n e^{j2(\Phi_h^{(m)} - \Phi_v^{(n)})} \right] \approx C_3 \left[\sum_i h_i^* v_i e^{j2\Phi_{DP}^{(i)}} \right], \quad (\text{A8})$$

$$C_3 = C_2 \frac{P_t G^2 \lambda^2}{(4\pi)^2} = \frac{2^6 \ln 2 \lambda^4 R_0^2}{\pi^5 c \tau \Omega^2 |K_w|^2}. \quad (\text{A9})$$

The summation and time averaging in Eq. (A8) can be replaced by integration over the radar resolution volume:

$$R_{\text{hv}}^{(m)} = C_3 \int n \langle s_{\text{hh}}^* s_{\text{vv}} \rangle \frac{e^{-2(\Gamma_{\text{h}} + \Gamma_{\text{v}})}}{R^4} e^{j\Phi_{\text{DP}}} f^4(\theta, \phi) R^2 \sin\theta \, dr \, d\theta \, d\phi, \quad (\text{A10})$$

where brackets stand for ensemble averaging and n is the concentration of scatterers.

According to the definition of the cross-correlation coefficient ρ_{hv} ,

$$n \langle s_{\text{hh}}^* s_{\text{vv}} \rangle = n \rho_{\text{hv}} \langle |s_{\text{hh}}|^2 \rangle^{1/2} \langle |s_{\text{vv}}|^2 \rangle^{1/2} \quad (\text{A11})$$

and

$$n \langle |s_{\text{hh},\text{vv}}|^2 \rangle = \frac{\pi^4}{4\lambda^4} |K_{\text{w}}|^2 Z_{\text{h,v}} \quad (\text{Doviak and Zrnice 1993}). \quad (\text{A12})$$

Hence,

$$R_{\text{hv}}^{(m)} = \frac{16 \ln 2 R_0^2}{\pi c \tau \Omega^2} \int Z_{\text{h}}^{1/2} Z_{\text{v}}^{1/2} |\rho_{\text{hv}}| e^{-2(\Gamma_{\text{h}} + \Gamma_{\text{v}})} e^{j\Phi_{\text{DP}}} \frac{f^4(\theta, \phi)}{R^2} \sin\theta \, dr \, d\theta \, d\phi, \quad (\text{A13})$$

where $\Phi'_{\text{DP}} = \Phi_{\text{DP}} + \arg(\rho_{\text{hv}})$.

If variables $Z_{\text{h,v}}$, $\Gamma_{\text{h,v}}$, ρ_{hv} , and Φ_{DP} are constant within the radar resolution volume, then the measured covariance $R_{\text{hv}}^{(m)}$ is equal to its intrinsic value

$$R_{\text{hv}} = Z_{\text{h}}^{1/2} Z_{\text{v}}^{1/2} |\rho_{\text{hv}}| e^{-2(\Gamma_{\text{h}} + \Gamma_{\text{v}})} e^{j\Phi'_{\text{DP}}}, \quad (\text{A14})$$

because

$$\int \frac{f^4(\theta, \phi)}{R^2} \sin\theta \, dr \, d\theta \, d\phi = \frac{\pi c \tau \Omega^2}{16 \ln 2 R_0^2} \quad (\text{A15})$$

in the case of the Gaussian axisymmetric antenna pattern (Doviak and Zrnice 1993).

If the covariance R_{hv} varies within the radar resolution volume but its variation along the radial direction is neglected due to much smaller radial dimension of the radar volume compared to its transverse dimensions at longer ranges from the radar, then the general expression (A13) can be simplified as follows:

$$R_{\text{hv}}^{(m)} = \int R_{\text{hv}}(\theta, \phi) I(\theta, \phi) \, d\theta \, d\phi, \quad (\text{A16})$$

where

$$I(\theta, \phi) = \frac{1}{2\pi\sigma^2} \exp\left(-\frac{\theta^2 + \phi^2}{2\sigma^2}\right) \quad (\text{A17})$$

and $\sigma = \Omega/4(\ln 2)^{1/2}$.

REFERENCES

- Brandes, E. A., A. V. Ryzhkov, and D. S. Zrnice, 2001: An evaluation of radar rainfall estimates from specific differential phase. *J. Atmos. Oceanic Technol.*, **18**, 363–375.
- , G. Zhang, and J. Vivekanandan, 2002: Experiments in rainfall estimation with a polarimetric radar in a subtropical environment. *J. Appl. Meteor.*, **41**, 674–685.
- Bringi, V. N., and V. Chandrasekar, 2001: *Polarimetric Doppler Weather Radar: Principles and Applications*. Cambridge University Press, 636 pp.
- Doviak, R. J., and D. S. Zrnice, 1993: *Doppler Radar and Weather Observations*. 2d ed. Academic Press, 562 pp.
- , V. Bringi, A. V. Ryzhkov, A. Zahrai, and D. S. Zrnice, 2000: Considerations for polarimetric upgrades to operational WSR-88D radars. *J. Atmos. Oceanic Technol.*, **17**, 257–278.
- Giangrande, S. E., and A. V. Ryzhkov, 2003: The quality of rainfall estimation with the polarimetric WSR-88D radar as a function of range. Preprints, *31st Int. Conf. on Radar Meteorology*, Seattle, WA, Amer. Meteor. Soc., 357–360.
- , —, and J. Krause, 2005: Automatic detection of the melting layer with a polarimetric prototype of the WSR-88D radar. Preprints, *32d Conf. on Radar Meteorology*, Albuquerque, NM, Amer. Meteor. Soc., CD-ROM, 11R.2.
- Gosset, M., 2004: Effect of nonuniform beam filling on the propagation of radar signals at X-band frequencies. Part II: Examination of differential phase shift. *J. Atmos. Oceanic Technol.*, **21**, 358–367.
- Herzogh, P. H., and R. E. Carbone, 1984: The influence of antenna illumination function characteristics on differential reflectivity measurements. Preprints, *22d Conf. on Radar Meteorology*, Zurich, Switzerland, Amer. Meteor. Soc., 281–286.
- Le Bouar, E., J. Testud, and T. D. Keenan, 2001: Validation of the rain profiling algorithm “ZPHI” from the C-band polarimetric weather radar in Darwin. *J. Atmos. Oceanic Technol.*, **18**, 1819–1837.
- Loney, M., D. Zrnice, J. Straka, and A. Ryzhkov, 2002: Enhanced polarimetric radar signatures above the melting level in a supercell storm. *J. Appl. Meteor.*, **41**, 1179–1194.
- May, P., T. D. Keenan, D. Zrnice, L. Carey, and S. Rutledge, 1999: Polarimetric radar measurements of tropical rain at 5-cm wavelength. *J. Appl. Meteor.*, **38**, 750–765.
- Meischner, P., Ed., 2004: *Weather Radar: Principles and Advanced Applications*. Springer, 337 pp.
- Pointin, Y. C., C. Ramond, and J. Fournet-Fayard, 1988: Radar differential reflectivity: A real-case evaluation of errors induced by antenna characteristics. *J. Atmos. Oceanic Technol.*, **5**, 416–423.

- Ryzhkov, A. V., 2005: On the use of differential phase for polarimetric rainfall measurements. A new approach to K_{DP} estimation. Preprints, *32d Conf. on Radar Meteorology*, Albuquerque, NM, Amer. Meteor. Soc., CD-ROM, P9R.8.
- , and D. Zrníc, 1998: Beamwidth effects on the differential phase measurements of rain. *J. Atmos. Oceanic Technol.*, **15**, 624–634.
- , and D. S. Zrníc, 2005: Radar polarimetry at S, C, and X bands: Comparative analysis and operational implications. Preprints, *32d Conf. on Radar Meteorology*, Albuquerque, NM, Amer. Meteor. Soc., CD-ROM, 9R.3.
- , T. J. Schuur, D. W. Burgess, S. Giangrande, and D. S. Zrníc, 2005a: The Joint Polarization Experiment: Polarimetric rainfall measurements and hydrometeor classification. *Bull. Amer. Meteor. Soc.*, **86**, 809–824.
- , S. E. Giangrande, and T. J. Schuur, 2005b: Rainfall estimation with a polarimetric prototype of the WSR-88D radar. *J. Appl. Meteor.*, **44**, 502–515.